

Matrix density regulates adipocyte phenotype

Alexander Ky^a, Atticus J. McCoy ^b, Carmen G. Flesher ^{a,c}, Nicole E. Friend ^b, Jie Li^a, Kore Akinleye^a, Christopher Patsalis ^{d,e}, Carey N. Lumeng ^{f,g,h}, Andrew J. Putnam ^b, and Robert W. O'Rourke ^{a,i}

^aDepartment of Surgery, University of Michigan, Ann Arbor, MI, USA; ^bDepartment of Biomedical Engineering, University of Michigan, Ann Arbor, MI, USA; ^cGraduate Program, University of Pennsylvania, Philadelphia, PA, USA; ^dDepartment of Internal Medicine, University of Michigan, Ann Arbor, MI, USA; ^eDepartment of Bioinformatics, University of Michigan, Ann Arbor, MI, USA; ^fDepartment of Pediatrics and Communicable Diseases, University of Michigan, Ann Arbor, MI, USA; ^gGraduate Program in Immunology, University of Michigan, Ann Arbor, MI, USA; ^hGraduate Program in Cellular and Molecular Biology, University of Michigan, Ann Arbor, MI, USA; ⁱDepartment of Surgery, Veterans Affairs Ann Arbor Healthcare System, Ann Arbor, MI, USA

ABSTRACT

Alterations of the extracellular matrix contribute to adipose tissue dysfunction in metabolic disease. We studied the role of matrix density in regulating human adipocyte phenotype in a tunable hydrogel culture system. Lipid accumulation was maximal in intermediate hydrogel density of 5 weight %, relative to 3% and 10%. Adipogenesis and lipid and oxidative metabolic gene pathways were enriched in adipocytes in 5% relative to 3% hydrogels, while fibrotic gene pathways were enriched in 3% hydrogels. These data demonstrate that the intermediate density matrix promotes a more adipogenic, less fibrotic adipocyte phenotype geared towards increased lipid and aerobic metabolism. These observations contribute to a growing literature describing the role of matrix density in regulating adipose tissue function.

ARTICLE HISTORY

Received 22 August 2023
Revised 28 September 2023
Accepted 29 September 2023

KEYWORDS

Adipocyte; adipogenesis; adipose tissue; matrix; hydrogel


Introduction


Adipose tissue dysfunction is an initiating trigger for metabolic disease in obesity, including type 2 diabetes. Features of adipose tissue associated with metabolic health include increased lipid storage and increased oxidative metabolism, while in metabolic disease, adipose tissue is characterized by increased inflammatory and immune responses, increased fibrosis, and increased glycolytic (anaerobic) metabolism [1–3]. Notably, similar phenotypic profiles distinguish depot-differences in adipose tissue. Subcutaneous adipose tissue (SAT), which is associated with metabolic health, is characterized by increased lipid storage and processing capacity, increased oxidative metabolism, and decreased inflammation and fibrosis, relative to visceral adipose tissue (VAT), an excess of which is linked to clinical metabolic disease [4–10].

Dysregulation of the extracellular matrix (ECM) plays a central role in adipose tissue dysfunction and metabolic disease pathogenesis [11–14]. Prior research by our group supports a role for ECM in regulating adipocyte metabolism in mice and humans [15,16], but underlying mechanisms are poorly defined. A dominant hypothesis is that elevated stiffness and/

or matrix density in fibrotic adipose tissue impairs adipocyte function, but efforts to correlate measures of human adipose tissue stiffness with disease are conflicting. Diabetic status in humans correlates with subcutaneous adipose tissue (SAT) stiffness measured by transcutaneous tonometry, but not with histologic measures of ECM deposition [17]. In another study, SAT stiffness did not change with bariatric surgery-induced weight loss despite the increased histologic signs of SAT collagen deposition and ECM remodelling [18]. We reported that diabetic status in humans correlates with increased visceral adipose tissue (VAT) stiffness measured with atomic force microscopy, but not with histologic measures of collagen content nor with macro-rheologic measures of tissue stiffness [19,20].

These conflicting data from study of native tissue mechanics suggest the need for *in vitro* models to define the role of matrix mechanics in regulating adipocyte function. Prior research by our group and others utilized ECM from native adipose tissue as a culture substrate [15,16,21], but such models do not permit dissection of the distinct roles of matrix mechanics and matrix protein composition in regulating cell function. Artificial matrix culture systems provide

CONTACT Robert W. O'Rourke  rorourke@med.umich.edu  Department of Surgery, Section of General Surgery, University of Michigan, 2210 Taubman Center-5343, 1500 E. Medical Center Drive Ann Arbor, MI, 48109-5343

 Supplemental data for this article can be accessed online at <https://doi.org/10.1080/21623945.2023.2268261>

© 2023 The Author(s). Published by Informa UK Limited, trading as Taylor & Francis Group. This is an Open Access article distributed under the terms of the Creative Commons Attribution-NonCommercial License (<http://creativecommons.org/licenses/by-nc/4.0/>), which permits unrestricted non-commercial use, distribution, and reproduction in any medium, provided the original work is properly cited. The terms on which this article has been published allow the posting of the Accepted Manuscript in a repository by the author(s) or with their consent.

a protein-free matrix that permit orthogonal engineering of stiffness independent of matrix protein composition [22–24]. These models demonstrate that, in both 2D and 3D culture models, increasing matrix stiffness impairs adipogenesis and mature adipocyte metabolic functions, but adipogenesis tends to be promoted to a greater extent in 3D matrices relative to 2D substrates [25–29]. Indeed, substantial prior research has studied adipogenesis in response to matrix stiffness in 2D culture [25–33], while data from 3D models, which arguably more accurately model the *in vivo* environment, are fewer.

Our goal was to evaluate the roles of matrix density and crosslinking in regulating human adipocyte metabolism. We studied adipocyte function in covalently cross-linked poly(ethylene glycol) vinyl sulphone (PEG-VS) 3D hydrogels, a model system that permits decoupling of initial matrix mechanical (e.g. stiffness) and biochemical (e.g. adhesive) properties, which are typically inseparable in native ECM materials. We hypothesized that decreasing matrix density and thereby initial stiffness would be associated with increasing adipogenesis and decreased fibrosis. Surprisingly, we found that lipid droplet size was maximal in 3D matrix of intermediate crosslinking/stiffness, but decreased in hydrogels of lesser or greater crosslinking/stiffness, with a corresponding enrichment in fibrotic gene pathway expression and decrease in lipid and oxidative metabolic gene transcription at the lowest levels of matrix density. These data suggest that an optimal point of 3D matrix density promotes adipogenesis, and that lower degrees of matrix density promote fibrotic gene expression with accompanying detrimental effects on adipocyte metabolism, possibly by permitting greater degrees of cell spreading. These observations have important implications for our understanding of matrix-adipocyte interactions in the context of metabolic disease.

Methods

Human subjects

Informed consent was obtained with Institutional Review Board approval at the University of Michigan and Veterans Affairs Ann Arbor Healthcare System under guidelines consistent with the 1964 Declaration of Helsinki and the 1974 Belmont Report. VAT from the greater omentum and SAT from the abdominal wall were collected from subjects with obesity (body mass index (BMI) ≥ 35) at the beginning of bariatric surgery, placed on ice and transported back to the laboratory for immediate processing. Tissues from 10 subjects were studied, five males and five females. Due to limitations

in cells, cells from subsets of subjects were used for different experiments and details in figure legends. All subjects were non-diabetic, defined by no clinical history of diabetes and HbA1c $< 5.7\%$ per American Diabetes Association criteria. Mean age = 36 y, standard deviation (s.d.) = 9; mean BMI = 44 kg/m², s.d. = 3; mean haemoglobin A1c = 5.3%, s.d. = 0.3.

Adipose tissue stromal cell (ASC) isolation

Isolation of ASC was performed as described [34]. Briefly, the adipose tissue was digested with Type II collagenase (2 mg/mL in PBS/2% BSA, Life Technologies Inc., Carlsbad, CA, USA) at 37°C, 60 min, centrifuged 250rcf, the stromal-vascular cell pellet retrieved, plated overnight, and adherent cells passaged three times to enrich for ASC, which were frozen in DMEM/F12, 15% foetal calf serum, 10% DMSO in liquid nitrogen until use.

PEG-VS hydrogel fabrication, cell culture

Poly(ethylene glycol) vinyl sulphone (PEG-VS) hydrogels were formed using 4-arm, 20 kDa poly(ethylene glycol) vinyl sulphone (JenKem Technology USA, Inc, Plano, TX, USA), a thiol-containing adhesive ligand peptide Ac-CGRGDS-NH₂ ('RGD'), and a dithiol-containing matrix metalloproteinase-sensitive crosslinking peptide Ac-GCRDVPMS↓MRGGDRCG-NH₂ ('VPMS'; AAPPTec, Louisville, KY, USA). Both RGD and VPMS have *N*-terminal acetylation and *C*-terminal amidation. PEG-VS was dissolved in ddH₂O, filtered through 0.22 μ m filters (Sigma-Aldrich, St. Louis, MO), aliquoted, lyophilized for 48 hr, and stored in a desiccator at -20°C . RGD and VPMS were dissolved in 25 mM acetic acid, filtered through 0.22 μ m filters, aliquoted, lyophilized for 48 hr, and stored in a desiccator at -20°C . The precise thiol content of each batch of peptide aliquots was determined using Ellman's reagent (ThermoFisher Scientific Inc., Waltham, MA, USA). For each experiment, PEG-VS, RGD, and VPMS aliquots were dissolved in HEPES (100 mM, pH 8.63, 20°C) to reach desired concentrations. 3 wt. %, 5 wt. %, and 10 wt. % PEG-VS gels were fabricated. RGD was conjugated to PEG-VS for 20 min at RT to achieve a final concentration of 0.5 mM RGD for all gel formulations. PEG-VS and RGD were further diluted to desired concentrations in HEPES. Ninety per cent or 100% of the remaining PEG-VS arms were crosslinked with VPMS for gel formation. The solution was vortexed, 50 μ L was pipetted into a 1 mL syringe (ThermoFisher Scientific Inc., Waltham, MA, USA) with the needle end cut off, and the hydrogel precursor

solution allowed to gel for 1 hr, 37°C in a sealed 50 mL conical tube. For cell-laden hydrogels, the precursor solution was used to resuspend a cell pellet of ASC to achieve a final cell density of 1×10^6 cells/mL. After the incubation at 37°C, hydrogels were ejected into 2 mL of differentiation media (DMEM:F12 + 10 mg/L transferrin, 33 μ M biotin, 0.5 μ M human insulin, 17 μ M pantothenate, 100 nM dexamethasone, 2 nM 3,3',5-Triiodo-L-thyronine sodium salt, 1 μ M ciglitazone, 540 μ M Isobutyl-1-methylxanthine), which was changed after day 1 then replaced every 2 d for 14 d. Acellular hydrogels were cultured in medium under similar conditions to determine the influence of exogenous medium on hydrogel degradation.

Hydrogel shear storage moduli (G') were measured on day 1 (to allow for overnight swelling) and on day 14 using an AR-G2 rheometer (TA Instruments, New Castle, DE, USA) between an 8-mm measurement head and a Peltier stage heated to 37°C. The Peltier plate and measurement head were covered with P800 sandpaper to reduce slippage. The shear storage modulus was averaged over a 1-min time sweep measured at 37°C, 5% strain amplitude, 1 rad/s frequency, and either 0.05 N normal force or a minimum gap height of 1000 μ m, if hydrogels were too soft to reach the target normal force.

Lipid droplet staining, imaging, quantification

After 14 d of differentiation, hydrogels containing differentiated mature adipocytes were fixed with 1 mL of zinc formalin (Z-Fix, Fisher Scientific Inc., Hampton, NH, USA, Cat#NC9378601) 10 min, 25°C, rinsed three times with PBS, and stored at 4°C in PBS prior to staining and imaging. For staining, the gels were incubated 20 min, 25°C with 500 μ L of blocking buffer (0.1% Triton-X-100 in PBS) 10 min, 25°C. Five hundred microlitres of 1% BSA in PBS was added per well for 20 min, 25°C. Blocking buffer was removed and 500 μ L of 1% BSA in PBS containing 25 μ L/mL Phalloidin (green; Invitrogen Inc., Waltham, MA, USA #A12379) was added to each well for 30 min, 25°C with wells protected from light, then removed, and hydrogels were washed twice with PBS. Five hundred microlitres of LipidTox (1:400; red; Invitrogen Inc., Waltham, MA, USA Cat#HS4476) in PBS, was added to each well for 30 min at 25°C, covered in foil, then removed, and gels were washed twice with PBS. Five hundred microlitres of 1 μ g/mL DAPI (blue; ThermoFisher Scientific, Inc., Waltham, MA, USA Cat#D1306) in PBS was added to each well, 10 min, 25°C, covered in foil, then removed, and gels were washed twice with PBS. One millilitre of PBS was

added to each well to cover the gels to prevent drying. Plates were covered in foil and stored at 4°C until imaging.

For imaging, gel pucks were cut in half using a sterile scalpel and placed cut-side down on a glass bottom 24-well plate such that the middle of the puck could be imaged. Spinning disk confocal microscopy (Nikon Corp., Tokyo, Japan) was used at 20 \times and 4–8 images were taken per hydrogels, resulting in 4–8 cells per gel (some images may contain more than 1 cell). Two-micrometre sections were taken to create a Z-stack from the bottom to the top of the adipocyte.

The image analysis was performed using Fiji image processing package [35]. The Z-stack was combined to a maximum intensity projection. Cell area was calculated by drawing borders around cells based on phalloidin stain, as during differentiation actin becomes localized to the periphery of the adipocyte. Lipid droplet sizing was performed by drawing borders on each lipid droplet and calculating area. This method captures more lipid droplets than by water shedding. Previous methods have used Fiji's water shedding method to calculate lipid droplet size. In 2D culture, this works well, but in 3D culture where lipid droplets may overlap each other, calculating lipid droplet area manually better captured the actual size of the lipid droplets. This is important when calculating the total lipid droplet area of a cell divided by that cell's area, as water shedding may underestimate the total lipid droplet area by not counting overlapping lipid droplets.

RNA sequencing (RNASeq)

After 14 d of culture, three 50 μ L hydrogels per experimental condition were rinsed with PBS, digested in 250 U/ml Collagenase IV, 45 min, 37°C, centrifuged, and the collagenase solution aspirated from the cell pellet. RNA was isolated using a QIAGEN QIAshredder and RNeasy mini kit (QIAGEN, Hilden, Germany). RNA concentration was measured using a ThermoScientific NanoDrop 2000 Spectrophotometer and RNA quality assessed using the BioAnalyzer (Agilent Inc., Santa Clara, CA, USA). Samples were stored at –80°C prior to RNASeq. For RNASeq, the SMART-Seq v4 PLUS kit (Takara Bio, Ann Arbor MI, USA) was used to prepare libraries from 2ng of RNA using 11 cycles of cDNA amplification and 15 cycles of library amplification per manufacturer's protocols. Final libraries were checked for quality and quantity by Qubit hsDNA (ThermoFisher Scientific, Inc., Waltham, MA, USA) and LabChip (Perkin Elmer, Waltham, MA, USA). Samples were pooled and sequenced on

the Illumina NovaSeq S4 paired-end 150 bp, according to manufacturer's recommended protocols. Data pre-processing, done by the University of Michigan Advanced Genomics core, utilized FastQC (v0.10.0) for quality control and the Tuxedo suite for alignment and quantification. Reads were aligned to the UCSC hg19 reference genome using TopHat [36,37], and gene quantification was done with Cufflinks [38]. Ensembl-ID gene sequences were used for annotation, and corresponding gene symbols were retrieved from biomaRt [39]. All subsequent analyses were performed in R statistical programming language. Count expression data was filtered to include features with a minimum of five counts in at least 50% of samples. Filtered data was collapsed using 2023 Ensembl Gene ID chip file and GSEA_R package (v1.2.0) published by the BROAD Institute [40]. If more than one Ensembl-ID corresponded to the same gene symbol, only the maximum value for each sample was kept. Paired-sample differential expression analysis was performed using DESeq2 (v1.8.3) [41] with default parameters. Gene set enrichment analysis was performed using fgsea R package (v1.24.0) [42]. Benjamini-Hochberg method was utilized for multiple-testing corrections.

Statistics

GraphPad Prism 9 was used for statistical analysis. Data normality was analysed by Shapiro-Wilk test. Comparisons between PEG% were performed using unpaired two-tailed t-tests. Experiments with more than one treatment were analysed by using one-way

ANOVA and multiple-comparison analysis (Tukey). Lipid droplet size frequency data from 3 wt.%, 5 wt.%, and 10 wt.% PEG were pooled into VAT or SAT depots. Descriptive statistics was run to generate quartiles for each depot. Small lipid droplet size was given a size range <1st quartile, medium between 2nd and 3rd quartile, large between 3rd and 4th quartile, and XL > 4th quartile. Quartiles were generated for each depot separately so as not to cause bias due to SAT lipid droplet tending to be larger than VAT lipid droplet. $p < 0.05$ was used as the threshold for statistical significance. Error bars in all graphs are the standard error of the mean.

Results

Rheologic properties of 3D hydrogels

We evaluated the rheologic properties of hydrogels in a range similar to prior-published data reporting the rheologic properties of adipose tissue [43–48]. Hydrogels with a PEG-VS density of 3 wt.%, 5 wt.%, and 10 wt.% exhibited shear storage moduli (G') ranging between 200 and 2,800 Pa. For acellular gels, only the 10 wt. % acellular gels manifested a decrease in shear modulus over the 14-d culture period (Figure 1a). Hydrogels seeded with VAT and SAT ASC had moduli significantly decreased over time in culture as ASC differentiated into adipocytes in all gel formulations, except VAT in 10% hydrogels (Figure 1b). These data support hydrogels of 3–10% as spanning a range of shear moduli similar to native adipose tissue, and suggest that gel degradation in culture is cell-mediated in 3% and 5% gels and is a combination of spontaneous and cell-mediated in 10% gels.

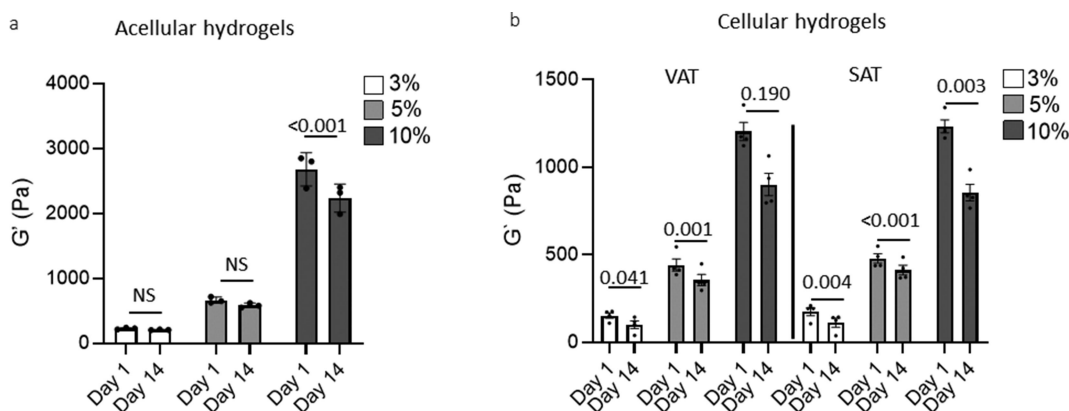


Figure 1. Hydrogel rheologic properties.

Shear storage moduli (G') of acellular hydrogels (a) and hydrogels seeded with ASC then differentiated into mature adipocytes (b) in tissue culture conditions on day 1 of culture, and on day 14 of culture. Statistically significant differences between experimental arms are denoted by p-values over indicated bars (ANOVA). Data from four patients, 2 M, 2F.

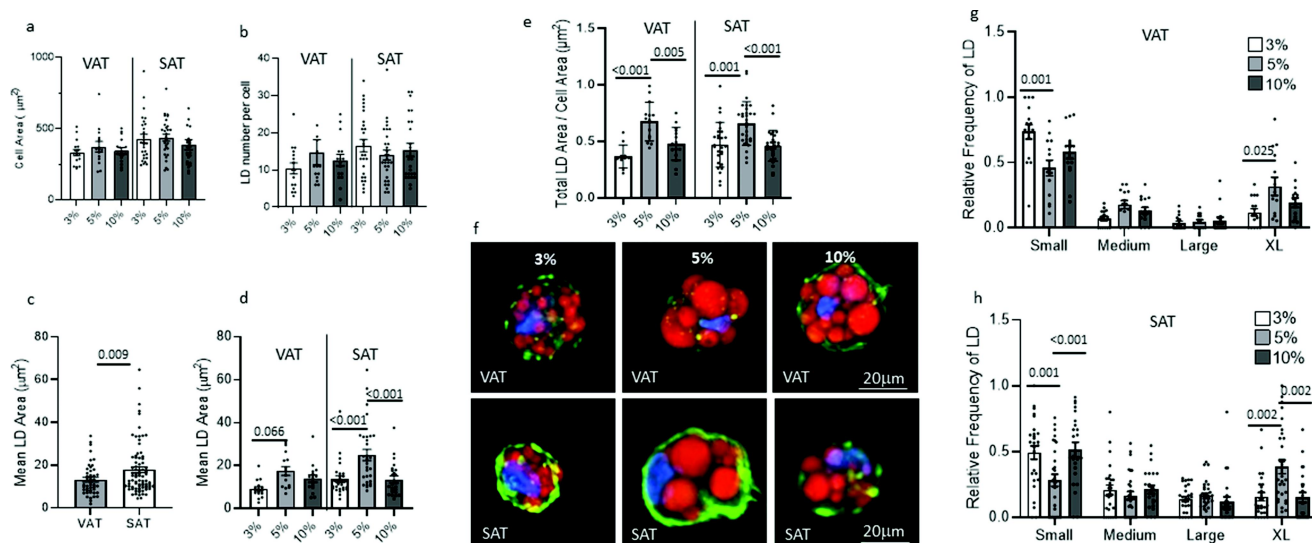


Figure 2. Hydrogel density regulates lipid droplet (LD) size independent of cell size or LD number.

a. Cell area (μm^2) of VAT or SAT mature adipocytes differentiated for 14 d in 3%, 5%, or 10% PEG-VS gels determined by Phalloidin staining and measured using FIJI. Each data-point represents the mean cell area (μm^2). No statistically significant differences were observed between experimental arms. b. Number of lipid droplets per mature adipocyte in 3%, 5%, or 10% PEG-VS gels determined by LipidTox staining and measured using FIJI. Each data-point represents the mean number of LD per cell. No statistically significant differences were observed between experimental arms. c. Mean lipid droplet area in mature adipocyte pooled from 3%, 5%, and 10% PEG-VS gels, separated by VAT and SAT. Each data-point represents the mean LD area per cell. Statistically significant differences between experimental arms denoted by p-values over indicated bars (ANOVA). d. Mean lipid droplet area in mature adipocyte in 3%, 5%, or 10% PEG-VS gels and separated by VAT and SAT. Each data-point represents the mean LD area per cell. Statistically significant differences between experimental arms denoted by p-values over indicated bars (ANOVA, Tukey's multiple comparisons test). e. Total lipid droplet area/cell area as a measure of lipid density in adipocytes, in 3%, 5%, or 10% PEG-VS gels, separated by VAT and SAT. Statistically significant differences between experimental arms denoted by p-values over indicated bars (ANOVA, Tukey's multiple comparison test). f. Representative confocal microscopy images of mature adipocytes in PEG-VS gels. g, h. Size frequency distribution of lipid droplet area in adipocytes differentiated for 14 d in 3%, 5%, or 10% PEG-VS gels quantified using confocal microscopy and FIJI. Small, Medium, Large, and X-Large droplets defined as $<9.2 \text{ mM}^2$, $9.2\text{--}14.5 \text{ mM}^2$, $14.6\text{--}18.6 \text{ mM}^2$, $>18.6 \text{ mM}^2$, respectively, for VAT, and $<9.8 \text{ mM}^2$, $9.8\text{--}14.7 \text{ mM}^2$, $14.8\text{--}22.6 \text{ mM}^2$, $>22.6 \text{ mM}^2$, respectively, for SAT. Each data-point represents the relative frequency of that size LD per cell. Statistically significant differences between experimental arms denoted by p-values over indicated bars (ANOVA, Tukey's multiple comparison test). Data from 7 to 8 cells per patient from four patients, 2 M, 2F.

Matrix density regulates lipid accumulation

We sought to determine the effect of hydrogel density on adipocyte lipid accumulation. ASC were differentiated for 14 d in 3%, 5%, or 10% PEG-VS gels, then lipid droplet morphology was assessed by confocal microscopy. No significant differences in cell area or mean number of lipid droplets per cell were observed between depots or PEG-VS% (Figure 2a, b). SAT adipocytes had larger mean lipid droplet area per cell relative to VAT adipocytes independent of gel density (i.e. data pooled from 3%, 5%, and 10% PEG-VS gels) (Figure 2c). In VAT adipocytes, the smaller lipid droplet area in 3% gels relative to 5% gels approached significance. Relative to 5% gels, SAT adipocytes in 3% or 10% PEG-VS gels had a smaller mean lipid droplet area. The total lipid droplet area per cell area, as a measure of lipid density in adipocytes, was greater in 5% relative to 3% and 10% gels in both VAT and SAT

adipocytes (Figure 2d, e.g). When stratified by lipid droplet size (Small, Medium, Large, X-Large), in VAT adipocytes we observed an increase in Small lipid droplets and a decrease in X-Large lipid droplets in 3% relative to 5% gels; in SAT adipocytes, smaller lipid droplet size in both 3% and 10% gels relative to 5% gels was the result of an increase in Small lipid droplets and a decrease in X-Large lipid droplets (Figure 2g, h). Similar trends were seen in both male and female subgroups when cells from males and females were analysed separately, suggesting no dramatic sex differences, but these results did not reach significance due to reduced sample size.

Together, these data demonstrate that gel density regulates lipid content in adipocytes by regulating lipid droplet size but not cell size or lipid droplet number, and that lipid content in adipocytes is maximal in gels of intermediate (5%) density, relative to gels of lower or higher density.

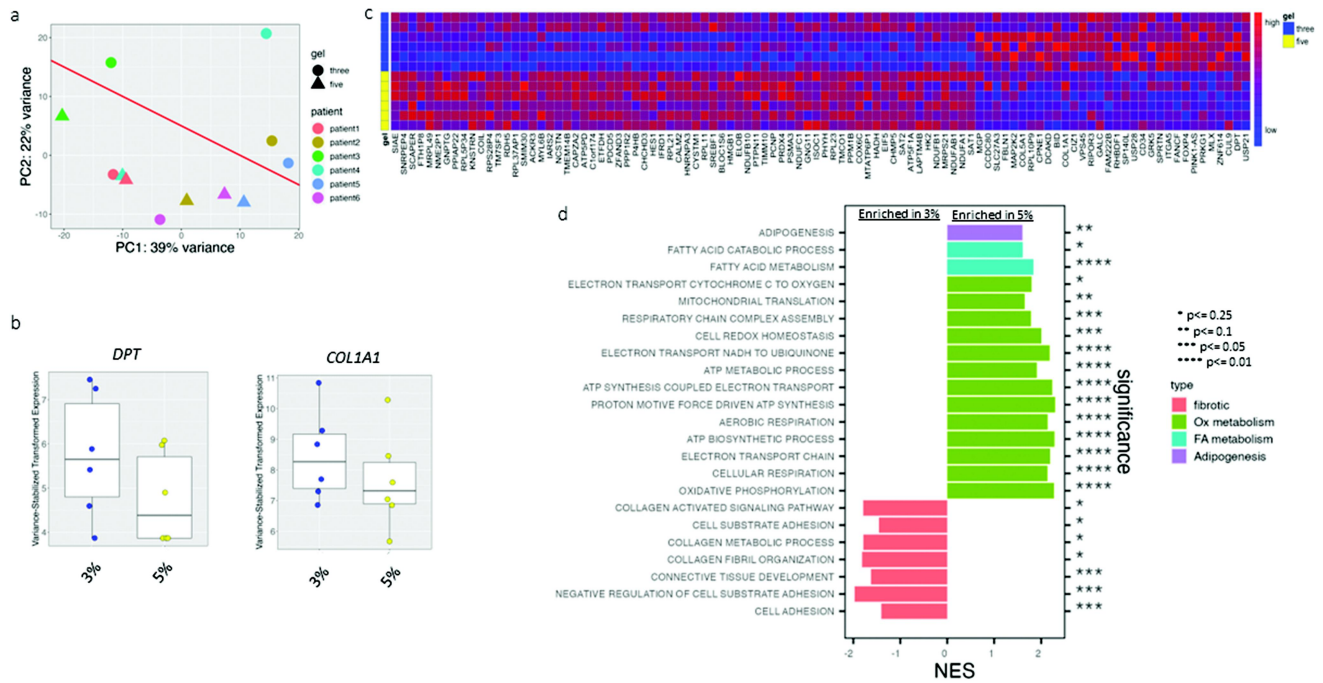


Figure 3. Hydrogel density regulates VAT adipocyte transcriptional phenotype.

a. PCA plot of RNA Seq data from all samples, showing gel % and individual patient identification (1–6). Diagonal line shows relative clustering by gel%. b. Boxplots of DEG (adjusted p-value <0.050) between adipocytes in 3% and 5% gels c. Heatmap of 100 top nominally significant DEG (unadjusted p-value <0.050) between adipocytes in 3% and 5% gels d. GSEA results comparing adipocytes in 3% and 5% gels. 3% is referent in this comparison, i.e. (+) normalized enrichment score (NES) designates pathway enriched in 5%, (-) NES designates pathway decreased in 5%. Query included Hallmark and C5- Gene Ontology-Biological Processes databases. Data from cells from six patients, 3 M, 3F.

Matrix density regulates the adipocyte transcriptome

We studied the adipocyte RNA transcriptome in response to hydrogel density by performing an initial discovery RNA-seq experiment using VAT adipocytes from six subjects with obesity (three males, three females) differentiated in 3% or 5% hydrogels (12 samples total). After processing and filtering out low-expressed genes, 9,581 genes were assessed. Principal component analysis (PCA) demonstrated reasonable clustering of data by gel per cent (3% vs 5%) (Figure 3a). Five hundred and eight genes had a p-value <0.05 prior to multiple-testing correction. The two genes were differentially expressed between groups after correction and at a threshold of $\alpha = 0.05$ (*COL1A1* (collagen type I alpha 1), and *DPT* (dermatopontin)), both increased in 3% gel relative to 5% gel (Figure 3b). A heatmap of the 100 top nominally significant differentially expressed genes (DEG) demonstrated visible differences between adipocytes in 3% vs. 5% gels (Figure 3c, Table 1S). GSEA pathway analysis [49–51] of all assessed genes revealed the upregulation of pathways associated with oxidative phosphorylation, electron transport, mitochondrial function, biosynthetic

processes, adipogenesis, and fatty acid metabolism in cells in 5% gels relative to the 3% gels. We also observed downregulation of pathways associated with fibrosis and extracellular matrix-cell interactions, i.e. cell adhesion pathways in 5% gel samples (Figure 3d, Supplemental Figure 1, Table 2S). The aforementioned metabolic processes were similarly upregulated in males and females when analysed separately; however, the fibrotic phenotype was not significantly downregulated in female samples, likely due to reduced sample size.

Together, these data support that an intermediate gel density (5%) induces a transcriptional phenotype characterized by increased adipogenesis and lipid and oxidative metabolism, while decreased gel density (3%) induces a fibrotic transcriptional phenotype with corresponding downregulation of pathways associated with adipogenesis and lipid and oxidative metabolism.

Depot-specific differences in the adipocyte transcriptome are preserved in hydrogel culture

To study depot-specific differences in the adipocyte transcriptome in the hydrogel environment, we

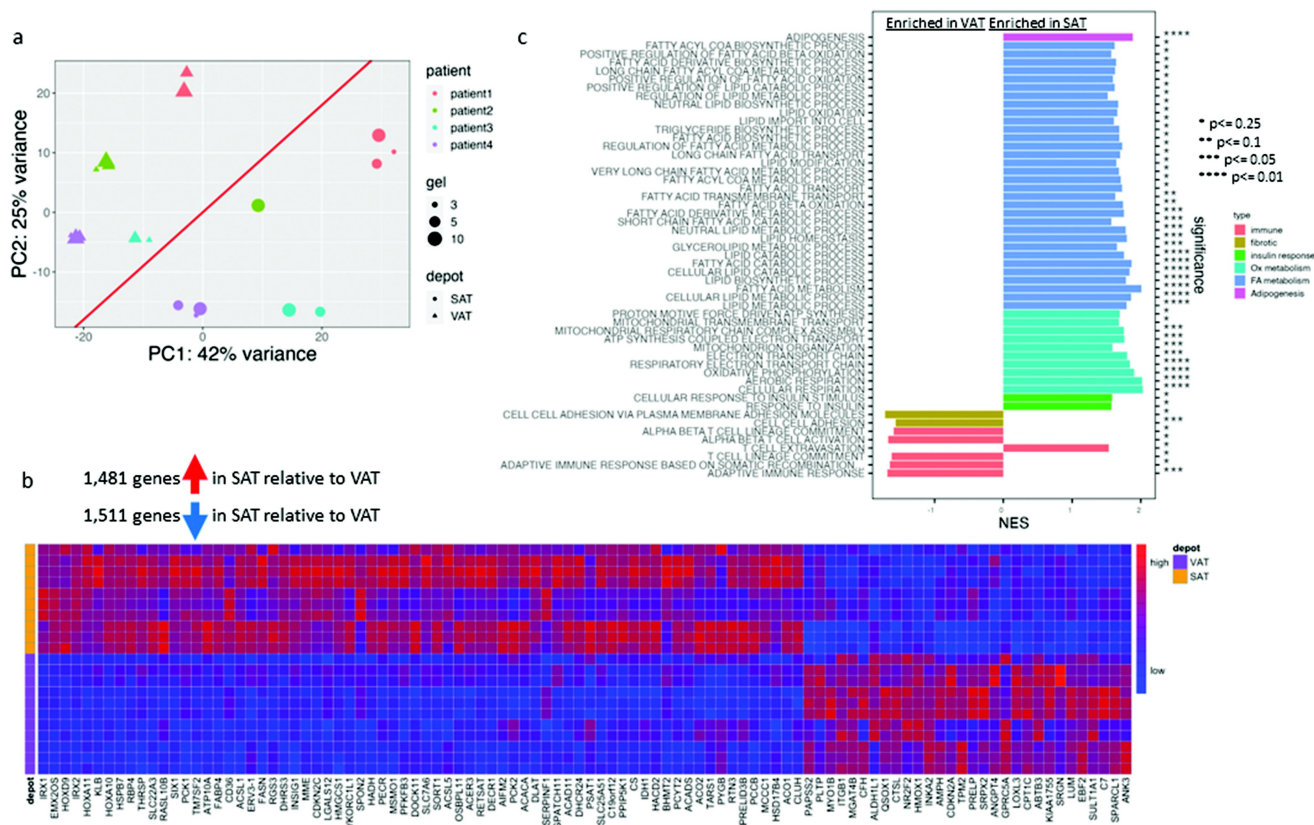


Figure 4. Depot-specific adipocyte transcriptional phenotypes in hydrogel culture.

a. PCA plot of RNA-Seq data from all samples, showing depot, gel%, and individual patient identification (1–6). Diagonal line shows relative clustering by depot. b. Heatmap of top 100 significant differentially expressed genes (adj p-value < 0.050) between VAT vs. SAT adipocytes in all hydrogels (3%, 5%, 10%). c. GSEA results comparing VAT vs. SAT adipocytes in all hydrogels (3%, 5%, 10%). VAT is referent in this comparison, i.e. (+) NES designates pathway enriched in SAT, (-) NES designates pathway decreased in SAT. Query included Hallmark and C5-Gene Ontology-Biological Processes databases. Data from cells from four patients, 2 M, 2F.

performed a second discovery RNA-seq experiment on a separate cohort of VAT and SAT adipocytes from four separate subjects with obesity (two males, two females) differentiated in 3%, 5%, or 10% hydrogels (24 samples total). When all cells (VAT and SAT) were analysed together, these data showed greater clustering by individual patient on PCA analysis, masking clustering by gel per cent (Figure 4a). Similar poor clustering by gel per cent was observed when data were analysed in VAT and SAT groups separately. These observations suggest that differences between individual patients in this second discovery dataset masked differences between gel per cent, likely due to the smaller number of subjects.

Despite this limitation, reasonable clustering of data by depot was observed in PCA when data from all gel weight per cents were studied (Figure 4a) permitting comparison of VAT and SAT transcriptomes in the hydrogel environment. After processing and filtering out lowly expressed genes, 7,692 genes were assessed.

When analysed independent of gel per cent, 1,481 genes were upregulated, and 1,511 genes were downregulated in SAT relative to VAT after multiple-testing corrections and at a threshold of $\alpha = 0.05$. Of the top 100 DEG's between SAT and VAT, SAT had increased expression of select genes involved in lipid metabolism (*CD36*, *FASN*, *FABP4*, *ACACA*, *ACAD11*) and decreased expression of select genes involved in fibrosis/ECM (*LUM*, *SPARCL1*, *ITGB1*, *LOXL3*) (Figure 4b, Table 3S). GSEA pathway analysis demonstrated that SAT adipocytes were enriched for pathways involved in lipid metabolism, while cell adhesion pathway was decreased by SAT adipocytes (Figure 4c, Supplemental Figure 2, Table 4S).

These findings are consistent with prior data supporting increased adipogenesis, lipid storage capacity, and oxidative metabolism and decreased fibrosis in SAT relative to VAT [4–10], and demonstrate that these established depot-specific phenotypes are preserved in hydrogel culture.

Discussion

We demonstrate that lipid droplet size and density in adipocytes is maximal in an intermediate stiffness hydrogel environment, and that hydrogel density of 5%, relative to 3%, promotes a more adipogenic transcriptional phenotype, while lower density gels of 3% promote fibrotic gene expression and decreased lipid and oxidative gene expression. Together, these data suggest that the inverse relationship between adipogenesis and matrix density is not linear, but rather, an intermediate matrix density promotes adipogenesis, lipid storage, and a metabolically beneficial adipocyte phenotype, above which lipid storage is reduced, and below which cells become more fibrotic and less adipogenic.

Much prior data regarding the relationship between matrix stiffness and adipogenesis is derived from 2D culture systems, but important qualitative differences exist between 2D and 3D environments with respect to adipogenesis. Hogrebe et al. found that gel stiffness regulates adipogenesis more robustly in 3D vs 2D culture, while Guo et al. found that stiffness did not regulate adipogenesis on 2D matrices [25,26]. In contrast, others have found that in 2D culture, matrix stiffness inhibits the adipogenesis of human ASC [28]. These observations support the importance of studying 3D systems to interrogate cell-matrix interactions. In contrast to 2D environments, 3D environments impose constraints on cell space and shape that increase with increasing matrix density. 3D matrices more effectively limit cell spreading, with increasing matrix stiffness and crosslinking imposing spatial constraints that affect cell function. As such, in 2D culture, cell spreading and matrix stiffness are correlated (i.e. stiffer substrates support more cell spreading) [45,52], but in most 3D cultures these variables are anticorrelated, as stiffer 3D matrices may constrain cell spreading by virtue of increased crosslinking and density of matrix that surrounds cells, whereas on a 2D substrate, this mechanical constraint is absent and cells only perceive stiffness of the underlying 2D matrix [23,53,54]. Such effects likely affect adipogenesis, evidenced by data demonstrating that 2D substrates engineered to mechanically constrain cells promote a round cell shape and potentiate adipogenesis independent of matrix stiffness [55]. Crosslinking and spatial constraints in the 3D system may explain our observations of maximal lipid accumulation and decreased fibrosis at intermediate gel density; gels below a density threshold, in our model 5%, may relieve cells of spatial constraints and permit cell spreading, leading to a more fibrotic, less adipogenic

phenotype. Precedent for an inverse relationship between matrix density and cell spreading exists in other systems [25].

We studied hydrogels ranging in stiffness (G') ranging from 150 Pa to 1200 Pa, a range that parallels the rheology of native adipose tissue. Using similar rheology methodology as ours, native adipose tissue has been found to have, on average, a G' value of 700–1100 Pa [43,44]. The elastic modulus, another common measure of stiffness, is related to storage modulus G' by $E = 2G'(1+\nu)$, where ν is Poisson's ratio, a measure of the ratio of transverse strain to axial strain (~ 0.5 for incompressible materials, a reasonable first approximation for elastic hydrogels) [45]. This equation puts our hydrogels in the elastic moduli range of 450–3600 Pa. Elastic moduli measurements of biological tissues range from 0.5 to 500 kPa [46], with native adipose tissue having an elastic modulus of 1–1.5 kPa [47,48]. This matches our mid-stiffness level with 5% PEG-VS ($E = 1.3$ kPa) with 3% and 10% PEG-VS gels spanning the lower and higher stiffness range (0.45 kPa and 3.6 kPa respectively).

Reciprocal effects of cells on matrix are an important feature of cell-matrix interactions. In some culture systems, stiffness decreases over time due to cell-mediated proteolysis of matrix components, and/or spontaneous degradation of hydrolytically susceptible crosslinks [56]. However, other studies show that cell-mediated remodelling of hydrogel biomaterials leads to increased matrix stiffness, possibly due to cells elaborating matrix molecules during culture [24,57,58]. The effect of cells on matrix remodelling leading to softening or stiffening is likely a function of cell phenotype as well as matrix composition. We observed a decrease in shear modulus in both acellular and cell-containing 10% hydrogels, but in 3% and 5% gels, we observed a decrease in shear modulus only in cellularized gels, suggesting that cell-mediated degradation is the dominant reason for decreased shear moduli in 3% and 5% gels, while both spontaneous and cell-mediated degradation leads to decreased shear moduli in 10% gels. Notably, while gel density regulated lipid droplet size, it did not regulate cell size (Figure 2a), which contrasts with other data demonstrating that the lower matrix density supports greater cell spreading in other cell types [54]. These observations suggest that at least in adipocytes, hydrogel density regulates cell phenotype independent of cell shape.

Our RNAseq experiments were designed as discovery experiments with a small number of patients, limiting the conclusions that can be drawn. Our RNAseq analysis of SAT adipocytes is underpowered, and therefore our transcriptomics results can only inform

regarding VAT adipocyte transcriptional responses. SAT adipocytes may exhibit different transcriptional responses to matrix mechanics, and larger studies will be necessary to define depot-specific transcriptional responses to matrix mechanics. Nonetheless, our data reveal novel findings. First, interpatient variability was substantial, masking the effects of gel per cent and other variables on the adipocyte transcriptome. Such interpatient variability is perhaps not surprising in a human cohort, but this observation suggests that large sample sizes will be necessary to generate statistically significant results with this methodology in human systems. This limitation was likely the reason why we observed only two genes that were statistically differentially regulated by gel density after multiple-testing correction. Both genes (*COL1A*, *DPT*) are ECM-related genes associated with fibrotic responses [59,60], reinforcing the increased fibrotic phenotype induced by lower gel density. Nonetheless, the paucity of significant DEG between groups despite the observed phenotypic differences in lipid droplet morphology suggests that our transcriptomics results must be interpreted with caution and support the need for designing studies with larger patient cohorts to define cell transcriptional responses. Second, despite these limitations and in line with the two observed DEG, we observed statistically significant enrichment of fibrosis-related gene pathways in 3% gels relative to 5% gels and enrichment of adipogenic and lipid and oxidative metabolic gene pathways in 5% gels relative to 3% gels. Increased lipid storage capacity, oxidative metabolism, and decreased fibrosis are features of metabolically healthy adipose tissue [1–3], and our data therefore suggest that 5% gels, relative to 3% gels, induce a beneficial metabolic phenotype in adipocytes, as a result of increased adipogenesis with a corresponding decrease in activation of fibrosis-related pathways. Finally, we observed differences in VAT and SAT adipocyte transcriptomes that support prior published functional data [4–10], namely increased lipid metabolism, oxidative metabolism, and adipogenesis in SAT relative to VAT across all gel densities, and increased fibrosis-related gene expression and immune/inflammatory related gene expression in VAT. These observations demonstrate that established depot-specific differences in adipocyte phenotype are maintained in the hydrogel environment.

Lipid storage capacity in adipocytes is an adaptive function, serving to buffer other tissues from excess nutrients, but excess lipid accumulation in adipocytes, or any cell for that matter, may become maladaptive and is associated with metabolic disease. We studied lipid storage, a key function of adipocytes, but other

metabolic processes may be regulated by matrix mechanics differently. Nonetheless, our transcriptomic data supports broad effects on adipocyte metabolism that overall support a metabolically beneficial phenotype in denser 5% hydrogels relative to less dense 3% gels, characterized by increased lipid buffering capacity, increased adipogenesis, increased lipid and oxidative metabolism, and decreased fibrosis. We studied ASC and adipocytes only from patients with obesity, and therefore our results cannot be extrapolated to cells from lean subjects. Future studies of cells from subjects across a wide range of BMI will be required to determine obesity-specific adipocyte responses to matrix mechanics. Our RNASeq experiments are exploratory, and further research will be necessary to fully define adipocyte phenotype in higher gel density, including 10%, and elucidate sex differences. Nonetheless, the current dataset provides novel insights into the regulation of metabolism in adipocytes and ASC by matrix mechanics.

We demonstrate that there exists an intermediate matrix density at which the adipocyte lipid accumulation is maximized, corresponding to 5% in our PEG-VS hydrogel system, which corresponds to the lower end of the mechanical properties of native adipose tissue. Gel densities below or above this threshold (i.e. 3%, 10% formulations) were associated with less lipid accumulation. Furthermore, at the lowest gel density (3%), relative to the intermediate gel density (5%), fibrotic gene expression pathways are enriched and lipid and oxidative metabolic gene pathways are decreased, suggesting that intermediate gel density supports a metabolically beneficial adipocyte phenotype. These results contribute to a growing body of literature that support the complex effects of extracellular matrix mechanics on adipocyte function, with implications for our understanding of adipose tissue dysfunction in disease.

Abbreviations

Adipose tissue stromal cells (ASC), body mass index (BMI); bovine serum albumin (BSA); differentially expressed genes (DEG); extracellular matrix (ECM); lipid droplet (LD); normalized enrichment score (NES); principal component analysis (PCA); RNA sequencing (RNAseq); subcutaneous adipose tissue (SAT); visceral adipose tissue (VAT).

Acknowledgments

Library prep and next-generation sequencing were carried out by the Advanced Genomics Core, University of Michigan.

Disclosure statement

No potential conflict of interest was reported by the author(s).

Funding

NIH grants R01DK115190 (RWO, CNL), R56DK132785 (RWO, CNL), R01DK090262 (CNL), Veterans Affairs Grant I01CX001811 (RWO).

Author contributions

Conceptualization: AJP, RWO; Data curation: AJM, AK, CGF, NEF, CP, CNL, AJP, RWO; Investigation: AK, AJM, CGF, NEF, AK, JL, KA; Methodology: AK, AJM, CGF, NEF, AK, JL, KA; Project administration: CNL, AJP, RWO; Funding acquisition: AJP, CNL, RWO; Writing, original draft: AJP, RWO; Writing, review & editing: all authors.

Competing interests

The authors declare no competing interests.

Data availability statement

Transcriptomics data from this study will be deposited in NIH-NIDDK dbGaP database as controlled access data. Requests for data from dbGap require application through the NIH dbGaP site, <https://dbgap.ncbi.nlm.nih.gov/aa/wga.cgi?page=login>. Other non-omics data from this study are derived from human subjects, who did not consent to deposition of non-omics data into databases other than dbGaP, and as such are not available for distribution, as such distribution would violate human subjects privacy and confidentiality.

ORCID

Atticus J. McCoy  <http://orcid.org/0000-0003-2736-8780>
 Carmen G. Flesher  <http://orcid.org/0009-0003-8984-8015>
 Nicole E. Friend  <http://orcid.org/0000-0001-5090-6538>
 Christopher Patsalis  <http://orcid.org/0009-0003-4585-0017>
 Carey N. Lumeng  <http://orcid.org/0000-0003-0303-6204>
 Andrew J. Putnam  <http://orcid.org/0000-0002-1262-4377>
 Robert W. O'Rourke  <http://orcid.org/0000-0002-4038-4198>

References

- [1] Carruthers NJ, Strieder-Barboza C, Caruso JA, et al. The human type 2 diabetes-specific visceral adipose tissue proteome and transcriptome in obesity. *Sci Rep.* 2021;11(1):17394. PMID: 34462518. doi: 10.1038/s41598-021-96995-0
- [2] Gómez-Serrano M, Camafeita E, López JA, et al. Differential proteomic and oxidative profiles unveil dysfunctional protein import to adipocyte mitochondria in obesity-associated aging and diabetes. *Redox Biol.* 2017;11:415–428. doi: 10.1016/j.redox.2016.12.013
- [3] Murri M, Insenser M, Bernal-Lopez MR, et al. Proteomic analysis of visceral adipose tissue in pre-obese patients with type 2 diabetes. *Mol Cell Endocrinol.* 2013;376(1–2):99–106. PMID: 23791845. doi: 10.1016/j.mce.2013.06.010
- [4] Gupta P, Lanca C, Gan ATL, et al. The Association between body composition using dual energy X-ray absorptiometry and type-2 diabetes: a systematic review and meta-analysis of observational studies. *Sci Rep.* 2019;9(1):12634. PMID: 31477766. doi: 10.1038/s41598-019-49162-5
- [5] Kahn D, Macias E, Zarini S, et al. Exploring visceral and subcutaneous adipose tissue secretomes in human obesity: implications for metabolic disease. *Endocrinology.* 2022;163(11):bqac140. PMID: 36036084. doi: 10.1210/endo/bqac140
- [6] Michaud A, Tordjman J, Pelletier M, et al. Relevance of omental pericellular adipose tissue collagen in the pathophysiology of human abdominal obesity and related cardiometabolic risk. *Int J Obes (Lond).* 2016;40(12):1823–1831. PMID: 27698346. doi: 10.1038/ijo.2016.173
- [7] Pafili K, Kahl S, Mastrototaro L, et al. Mitochondrial respiration is decreased in visceral but not subcutaneous adipose tissue in obese individuals with fatty liver disease. *J Hepatol.* 2022;77(6):1504–1514. PMID: 35988689. doi: 10.1016/j.jhep.2022.08.010
- [8] Porter SA, Massaro JM, Hoffmann U, et al. Abdominal subcutaneous adipose tissue: a protective fat depot? *Diabetes Care.* 2009;32(6):1068–1075. PMID: 19244087. doi: 10.2337/dc08-2280
- [9] Preis SR, Massaro JM, Robins SJ, et al. Abdominal subcutaneous and visceral adipose tissue and insulin resistance in the Framingham heart study. *Obesity (Silver Spring).* 2010;18(11):2191–2198. PMID: 20339361. doi: 10.1038/oby.2010.59
- [10] Raajendiran A, Krisp C, Souza DP, et al. Proteome analysis of human adipocytes identifies depot-specific heterogeneity at metabolic control points. *Am J Physiol Endocrinol Metab.* 2021;320(6):E1068–E1084. PMID: 33843278. doi: 10.1152/ajpendo.00473.2020.
- [11] Divoux A, Tordjman J, Lacasa D, et al. Fibrosis in human adipose tissue: composition, distribution, and link with lipid metabolism and fat mass loss. *Diabetes.* 2010;59(11):2817–2825. PMID: 20713683. doi: 10.2337/db10-0585
- [12] Henegar C, Tordjman J, Achard V, et al. Adipose tissue transcriptomic signature highlights the pathological relevance of extracellular matrix in human obesity. *Genome Biol.* 2008;9(1):R14. PMID: 18208606. doi: 10.1186/gb-2008-9-1-r14.
- [13] Lackey DE, Burk DH, Ali MR, et al. Contributions of adipose tissue architectural and tensile properties toward defining healthy and unhealthy obesity. *Am J Physiol Endocrinol Metab.* 2014;306(3):E233–46. doi: 10.1152/ajpendo.00476.2013
- [14] Muir LA, Neeley CK, Meyer KA, et al. Adipose tissue fibrosis, hypertrophy, and hyperplasia: correlations with diabetes in human obesity. *Obesity (Silver Spring).* 2016;24(3):597–605. PMID: 26916240. doi: 10.1002/oby.21377

- [15] Baker NA, Muir LA, Washabaugh AR, et al. Diabetes-specific regulation of adipocyte metabolism by the adipose tissue extracellular matrix. *J Clin Endo Metab.* 2017;102(3): 1–12. PMID: 28359093.
- [16] Strieder-Barboza C, Baker NA, Flesher CG, et al. Depot-specific adipocyte-extracellular matrix metabolic crosstalk in murine obesity. *Adipocyte.* 2020;9(1):89–96. PMID: 32272860. doi: 10.1080/21623945.2020.1749500
- [17] Abdennour M, Reggio S, Le Naour G, et al. Association of adipose tissue and liver fibrosis with tissue stiffness in morbid obesity: links with diabetes and BMI loss after gastric bypass. *J Clin Endocrinol Metab.* 2014;99(3):898–907. PMID: 24423338. doi: 10.1210/jc.2013-3253
- [18] Liu Y, Aron-Wisnewsky J, Marcelin G, et al. Accumulation and changes in composition of Collagens in subcutaneous adipose tissue after bariatric Surgery. *J Clin Endocrinol Metab.* 2016;101(1):293–304. PMID: 26583585. doi: 10.1210/jc.2015-3348
- [19] Juliar BA, Strieder-Barboza C, Karmakar M, et al. Viscoelastic characterization of diabetic and non-diabetic human adipose tissue. *Biorheology.* 2020;57(1):15–26. PMID: 32083565. doi: 10.3233/BIR-190234
- [20] Wenderott JK, Flesher CG, Baker NA, et al. Elucidating nanoscale mechanical properties of diabetic human adipose tissue using atomic force microscopy. *Sci Rep.* 2020;10(1):20423. PMID: 33235234. doi: 10.1038/s41598-020-77498-w
- [21] Pellegrinelli V, Heuvingh J, du Roure O, et al. Human adipocyte function is impacted by mechanical cues. *J Pathol.* 2014;233(2):183–195. PMID: 24623048. doi: 10.1002/path.4347
- [22] Beamish JA, Juliar BA, Cleveland DS, et al. Deciphering the relative roles of matrix metalloproteinase- and plasmin-mediated matrix degradation during capillary morphogenesis using engineered hydrogels. *J Biomed Mater Res B Appl Biomater.* 2019;107(8):2507–2516. doi: 10.1002/jbm.b.34341
- [23] Cruz-Acuña R, García AJ. Synthetic hydrogels mimicking basement membrane matrices to promote cell-matrix interactions. *Matrix Biol.* 2017;57-58:324–333. PMID: 27283894. doi: 10.1016/j.matbio.2016.06.002.
- [24] Juliar BA, Beamish JA, Busch ME, et al. Cell-mediated matrix stiffening accompanies capillary morphogenesis in ultra-soft amorphous hydrogels. *Biomaterials.* 2020;230:119634. doi: 10.1016/j.biomaterials.2019.119634
- [25] Högbe NJ, Gooch KJ. Direct influence of culture dimensionality on human mesenchymal stem cell differentiation at various matrix stiffnesses using a fibrous self-assembling peptide hydrogel. *J Biomed Mater Res A.* 2016;104(9):2356–2368. doi: 10.1002/jbm.a.35755
- [26] Guo Y, Qiao Y, Quan S, et al. Relationship of matrix stiffness and cell morphology in regulation of osteogenesis and adipogenesis of BMSCs. *Mol Biol Rep.* 2022;49(4):2677–2685. doi: 10.1007/s11033-021-07075-5
- [27] Xie J, Zhang D, Zhou C, et al. Substrate elasticity regulates adipose-derived stromal cell differentiation towards osteogenesis and adipogenesis through β -catenin transduction. *Acta Biomater.* 2018;79:83–95. doi: 10.1016/j.actbio.2018.08.018
- [28] Young DA, Choi YS, Engler AJ, et al. Stimulation of adipogenesis of adult adipose-derived stem cells using substrates that mimic the stiffness of adipose tissue. *Biomaterials.* 2013;34(34):8581–8588. doi: 10.1016/j.biomaterials.2013.07.103
- [29] Zohora FT, Aldebs AI, Nosoudi N, et al. Gene expression profiling of human adipose tissue stem cells during 2D versus 3D adipogenesis. *Cells Tissues Organs.* 2019;208(3–4):113–133. doi: 10.1159/000507187
- [30] Dupont S, Morsut L, Aragona M, et al. Role of YAP/TAZ in mechanotransduction. *Nature.* 2011;474(7350):179–183. doi: 10.1038/nature10137
- [31] Lee J, Abdeen AA, Tang X, et al. Matrix directed adipogenesis and neurogenesis of mesenchymal stem cells derived from adipose tissue and bone marrow. *Acta Biomater.* 2016;42:46–55. doi: 10.1016/j.actbio.2016.06.037
- [32] Piroli ME, Jabbarzadeh E. Matrix stiffness modulates mesenchymal stem cell sensitivity to geometric asymmetry signals. *Ann Biomed Eng.* 2018;46(6):888–898. doi: 10.1007/s10439-018-2008-8
- [33] Zhang T, Lin S, Shao X, et al. Regulating osteogenesis and adipogenesis in adipose-derived stem cells by controlling underlying substrate stiffness. *J Cell Physiol.* 2018;233(4):3418–3428. doi: 10.1002/jcp.26193
- [34] Baker NA, Muir LA, Lumeng CN, et al. Differentiation and Metabolic Interrogation of Human Adipocytes. *Methods Mol Biol.* 2017;1566:61–76. PMID: 28244041; PMCID: PMC5762179. doi: 10.1007/978-1-4939-6820-6
- [35] Schindelin J, Arganda-Carreras I, Frise E, et al. Fiji: an open-source platform for biological-image analysis. *Nat Methods.* 2012;9(7):676–682. doi: 10.1038/nmeth.2019
- [36] Trapnell C, Pachter L, Salzberg SL. TopHat: discovering splice junctions with RNA-Seq. *Bioinformatics.* 2009;25(9):1105–1111. doi: 10.1093/bioinformatics/btp120
- [37] Kim D, Pertea G, Trapnell C, et al. TopHat2: accurate alignment of transcriptomes in the presence of insertions, deletions and gene fusions. *Genome Biol.* 2013;14(4):R36. doi: 10.1186/gb-2013-14-4-r36
- [38] Trapnell C, Williams BA, Pertea G, et al. Transcript assembly and quantification by RNA-Seq reveals unannotated transcripts and isoform switching during cell differentiation. *Nat Biotechnol.* 2010;28(5):511–515. PMID: 20436464. doi: 10.1038/nbt.1621
- [39] Durinck S, Spellman PT, Birney E, et al. Mapping identifiers for the integration of genomic datasets with the R/Bioconductor package biomaRt. *Nat Protoc.* 2009;4(8):1184–1191. doi: 10.1038/nprot.2009.97
- [40] Subramanian A, Tamayo P, Mootha VK, et al. Gene set enrichment analysis: a knowledge-based approach for interpreting genome-wide expression profiles. *Proc Natl Acad Sci.* 2005;102(43):15545–15550. PMID: 16199517. doi: 10.1073/pnas.0506580102
- [41] Love MI, Huber W, Anders S. Moderated estimation of fold change and dispersion for RNA-seq data with DESeq2. *Genome Biol.* 2014;15(12):550. doi: 10.1186/s13059-014-0550-8

- [42] Korotkevich G, Sukhov V, Budin N, et al. Fast gene set enrichment analysis. *bioRxiv*. Published online February 1, 2021:060012. doi:10.1101/060012
- [43] Huber B, Borchers K, Tovar G, et al. Methacrylated gelatin and mature adipocytes are promising components for adipose tissue engineering. *J Biomat App*. 2016;30(6):699–710. doi: 10.1177/0885328215587450
- [44] Kochar A, Wu I, Mohan R, et al. A comparison of the rheologic properties of an adipose-derived extracellular matrix Biomaterial, lipoaspirate, calcium hydroxyapatite, and cross-linked Hyaluronic acid. *JAMA Facial Plast Surg*. 2014;16(6):405–409. doi: 10.1001/jamafacial.2014.480
- [45] Guimarães CF, Gasperini L, Marques AP, et al. The stiffness of living tissues and its implications for tissue engineering. *Nat Rev Mater*. 2020;5(5):351–370. doi: 10.1038/s41578-019-0169-1
- [46] Feig V, Tran H, Lee M, et al. Mechanically tunable conductive interpenetrating network hydrogels that mimic the elastic moduli of biological tissue. *Nat Commun*. 2018;9(2740). doi: 10.1038/s41467-018-05222-4
- [47] Borzacchiello A, Mayol L, Ramires PA, et al. Structural and rheological characterization of hyaluronic acid-based scaffolds for adipose tissue engineering. *Biomaterials*. 2007;28(30):4399–4408. doi: 10.1016/j.biomaterials.2007.06.007
- [48] Comley K, Fleck NA. A micromechanical model for the young's modulus of adipose tissue. *Int J Solids Struct*. 2010;47(21):2982–2990. doi: 10.1016/j.ijsolstr.2010.07.001
- [49] Liberzon A, Birger C, Thorvaldsdóttir H, et al. The molecular signatures database (MSigDB) hallmark gene set collection. *Cell Syst*. 2015;1(6):417–425. doi: 10.1016/j.cels.2015.12.004
- [50] The Gene Ontology Consortium, Aleksander SA, Balhoff J, et al. The gene Ontology knowledgebase in 2023. *Genetics*. 2023;224(1):iyad031.
- [51] Engler AJ, Sen S, Sweeney HL, et al. Matrix elasticity directs stem cell lineage specification. *Cell*. 2006;126(4):677–689. doi: 10.1016/j.cell.2006.06.044
- [52] Morgan FLC, Fernández-Pérez J, Moroni L, et al. Tuning hydrogels by mixing dynamic cross-linkers: enabling cell-instructive hydrogels and Advanced bioinks. *Adv Healthc Mater*. 2022;11(1):e2101576. PMID: 34614297. doi: 10.1002/adhm.202101576
- [53] Ghajar CM, Chen X, Harris JW, et al. The effect of matrix density on the regulation of 3-D capillary morphogenesis. *Biophys J*. 2008;94(5):1930–1941. PMID: 17993494. doi: 10.1529/biophysj.107.120774.
- [54] Khetan S, Guvendiren M, Legant WR, et al. Degradation-mediated cellular traction directs stem cell fate in covalently crosslinked three-dimensional hydrogels. *Nat Mater*. 2013;12(5):458–465. doi: 10.1038/nmat3586
- [55] Kilian KA, Bugarija B, Lahn BT, et al. Geometric cues for directing the differentiation of mesenchymal stem cells. *Proc Natl Acad Sci, USA*. 2010;107(11):4872–4877. PMID: 20194780. doi: 10.1073/pnas.0903269107
- [56] Hunt NC, Smith AM, Gbureck U, et al. Encapsulation of fibroblasts causes accelerated alginate hydrogel degradation. *Acta Biomater*. 2010;6(9):3649–3656. doi: 10.1016/j.actbio.2010.03.026
- [57] Kesselman D, Kossover O, Mironi-Harpaz I, et al. Time-dependent cellular morphogenesis and matrix stiffening in proteolytically responsive hydrogels. *Acta Biomater*. 2013;9(8):7630–7639. PMID: 23624218. doi: 10.1016/j.actbio.2013.04.030
- [58] Friend NE, McCoy AJ, Stegemann JP, et al. A combination of matrix stiffness and degradability dictate microvascular network assembly and remodeling in cell-laden poly(ethylene glycol) hydrogels. *Biomaterials* PMID: 36812843. 2023;295:122050. doi: 10.1016/j.biomaterials.2023.122050
- [59] Unamuno X, Gómez-Ambrosi J, Ramírez B, et al. Dermatopontin, a novel adipokine promoting adipose tissue extracellular matrix remodeling and inflammation in obesity. *J Clin Med*. 2020;9(4):1069. PMID: 32283761. doi: 10.3390/jcm9041069
- [60] Jääskeläinen I, Petäistö T, Mirzarazi Dahagi E, et al. Collagens regulating adipose tissue formation and functions. *Biomedicines*. 2023;11(5):1412. PMID: 37239083. doi: 10.3390/biomedicines11051412